Supporting Information

Directly Monitoring the Active Sites of Charge Transfer in Heterocycles in Situ and in Real Time

Shuji Ye,[a,*] Junjun Tan,[a] Kangzhen Tian,[a] Chuanzhao Li,[a] Jiahui Zhang,[a] Yi Luo[a],

[a] Hefei National Laboratory for Physical Sciences at the Microscale, and Synergetic Innovation Center of Quantum Information & Quantum Physics, University of Science and Technology of China, Hefei, Anhui 230026, China

1. Materials and substrate cleaning

Lumiflavin (LF, purity ≥ 98%), riboflavin (RF, purity ≥ 98%), flavin mononucleotide (FMN, purity ≥ 98%), and flavin adenine dinucleotide (FAD, purity ≥ 98%), $CaCl_2$(purity ≥ 99.8%), D_2O(purity ≥ 99.9%) were purchased from Sigma-Aldrich. DMSO (purity ≥99.0%) and Sodium hyposulfite ($Na_2S_2O_4$, purity >88.0%) were purchased from Sinopharm Chemical Reagent Co., Ltd. CaF_2 prisms were purchased from Chengdu Ya Si Opteoelectronics Co., Ltd (Chengdu, China). All of the chemicals were used as received. CaF_2 prisms were thoroughly cleaned using a procedure with several steps: They were first soaked in toluene for 24 h and then sonicated in soap detergent solution for 0.5 h. After that, they were rinsed with deionized (DI) water before soaking in methanol for 10 minutes. All of the prisms were then rinsed thoroughly with an ample amount of ultrapure water from a Milli-Q reference system (Millipore, Bedford, MA) and cleaned inside Harrick plasma chamber for 10 min immediately before preparing samples on them. Substrates were tested using IV-SFG and no signal from contamination was detected.

2. IV-SFG and IIV-SFG principles

The principles of IV-SFG and IIV-SFG have been extensively discussed elsewhere.[1-10] IV-SFG is based on a coherent second-order nonlinear process while IIV-SFG is based on a coherent third-order nonlinear process. In a typical IV-SFG experiment, two pulsed laser beams, one with

a fixed frequency in the visible frequency range (ω_{Vis}), and one with a tunable frequency in the infrared frequency range (ω_{IR}), are overlapped spatially and temporally on the sample. The IV-SFG signal is generated at the sum frequency of the two input beams by the nonlinear process (Eq.S1), and its specific directions of propagation are given by the phase-matching conditions of the wave vectors($\vec{k}$) (Eq.S2):

$$\omega_{SFG} = \omega_{Vis} + \omega_{IR} \tag{S1}$$

$$\vec{k}_{SFG} = \vec{k}_{Vis} + \vec{k}_{IR} \tag{S2}$$

The resonant part of $\chi^{(2)}$ that gives rise to the IV-SFG signal is given by[1,9]

$$\chi^{(2)}_{IV-SFG}(\omega_{Vis}, \omega_{IR}) = \frac{2}{\mathrm{h}}\left\{\frac{(\partial\alpha/\partial Q_1)_0(\partial\mu/\partial Q_1)_0}{(\omega_{IR} - \omega_0 + i\Gamma_{vg})}\right\}\left|\langle g|Q_1|v\rangle\right|^2 \tag{S3}$$

Similarly, based on energy and momentum conservation, IIV-SFG has the following relationships:

$$\omega_{IIV-SFG} = \omega_{Vis} + \omega_{IR1} + \omega_{IR2} \tag{S4}$$

$$\Delta\vec{k} = \vec{k}_{Vis} + \vec{k}_{IR1} + \vec{k}_{IR2} - \vec{k}_{IIV-SFG} \tag{S5}$$

According to Eqs.S1-S2 and S4-S5, the wavelengths and propagation directions of IV-SFG and IIV-SFG signal can be determined by knowing the wavelengths and incidence angles of visible and IR beams. It need mention that the phase-matching condition in IV-SFG is the momentum conservation in the direction parallel with the surface, while the momentum conservation in IIV-SFG is different due to its $\chi^{(3)}$ process. The IIV-SFG pathway cannot be perfectly phase-matched in systems with normal dispersion because the indices of refraction (higher index at higher frequency) make the $\vec{k}_{IIV-SFG}$ output wave vector larger than the $\vec{k}_{Vis} + \vec{k}_{IR1} + \vec{k}_{IR2}$ nonlinear polarization wave vector. Nevertheless, under triply resonant conditions, IIV-SFG has high output intensities because the three resonance enhancements are multiplicative and create a large nonlinear gain over a path length shorter than the inverse of their phase-mismatch, Δk.[6-9]

The theoretical description of IIV-SFG process has been given by Cho and Wright et al.[6-9] In the IIV-SFG process, the pathway ($gg \rightarrow \nu g \rightarrow (\nu+\nu')g \rightarrow eg$) represents a unique coherence pathway where the first IR pulse (ω_{IR1}) excites fundamental vibrational modes, the second IR pulse (ω_{IR2}) excites overtone and combination band modes, and the visible pulse (ω_{Vis}) excites

the final electronic coherent state which generates a coherent Raman transition, returning the system to the ground state.[6-9] The third-order susceptibility for IIV-SFG is given as[6-9]

$$\chi^{(3)}_{IIV-SFG}(\omega_{IR1},\omega_{IR2},\omega_{vis}) = \frac{1}{\mathrm{h}^2}\sum_{v,v+v'}\frac{\langle g\,|\,\alpha\,|\,(v+v')\rangle\langle(v+v')\,|\,\mu^{(2)}\,|\,v\rangle\langle(v)\,|\,\mu^{(1)}\,|\,\mathrm{g}\rangle}{(\omega_{IR1}+\omega_{IR2}-2\omega_0+i\Gamma_{(v+v')\mathrm{g}})(\omega_{IR1}-\omega_0+i\Gamma_{vg})} \qquad \text{(S6)}$$

where $\mu^{(i)}$ is the dipole moment in the electronic ground state, α is the conventional optical polarizability and i represents the *i*th external field. $|\mathrm{n}\rangle$ represents the vibrational state shown in Figure 1A. The dephasing constant of the coherence state $|\mathrm{m}\rangle\langle\mathrm{n}|$ is denoted as Γ_{mn}.[9] According to the theoretical description given by Cho,[9,10] when the lowest-order contributions to the third-order susceptibility are considered, the resonant part of $\chi^{(3)}$ originates from the vibrational anharmonicity($\chi^{(3)}_{AN}$) and higher-order nonlinearities of the polarizability and dipole moment of the chromophore($\chi^{(3)}_{NL}$), respectively.[9,10] For our case, the vibrational temperatures are much greater than the experimental temperature, and $\omega_{\mathrm{IR1}} = \omega_{\mathrm{IR2}}$, $\chi^{(3)}_{AN}$ and $\chi^{(3)}_{NL}$ can be simplified as[9,10]

$$\chi^{(3)}_{AN}(\omega_{IR},\omega_{IR},\omega_3) = \frac{1}{\mathrm{h}^2}\sum_{j=1}^{2}\left\{\frac{(\partial\alpha/\partial Q_j)_0(\partial\mu^{(2)}/\partial Q_1)_0(\partial\mu^{(1)}/\partial Q_1)_0}{(2\omega_{IR1}-2\omega_0+i\Gamma_{(v+v)g})(\omega_{IR1}-\omega_0+i\Gamma_{vg})}\right\}\langle g|Q_j|(v+v')\rangle\langle(v+v')|Q_1|v\rangle\langle v|Q_1|g\rangle \qquad \text{(S7)}$$

$$\chi^{(3)}_{NL}(\omega_{IR},\omega_{IR},\omega_3) = \frac{1}{2\mathrm{h}^2}\left\{\frac{(\partial^2\alpha/\partial Q_1^2)_0(\partial\mu^{(2)}/\partial Q_1)_0(\partial\mu^{(1)}/\partial Q_1)_0}{(2\omega_{IR1}-2\omega_0+i\Gamma_{(v+v')g})(\omega_{IR1}-\omega_0+i\Gamma_{vg})}\right\}\langle g|Q_1^2|(\mathrm{v}+\mathrm{v}'))\rangle\langle(v+v')|Q_1|v\rangle\langle v|Q_1|g\rangle \qquad \text{(S8)}$$

where Q_j represents the vibrational coordinate of molecules j. Eqs.S7-S8 indicate that (i) those vibrational modes that are IIV-SFG active must be both infrared and Raman active, and (ii) that mode should be either anharmonic or the second-order nonlinear terms of α should not be negligible.[6-10]

According to the selection rule for the Raman scattering, transition with $\Delta v \neq 1$ is very weak for the non-resonant case. It can occur often because of Fermi resonance of the overtones and combination bands with Raman-active fundamental modes.[6-9] However, for the resonant Raman scattering, the absorption cross section values of overtone and combination band transitions is significantly amplified due to the important contribution of the Franck-Condon factors and the higher-order components of the Herzberg-Teller expansion.[6, 7, 11, 12] Therefore, in the IIV-SFG process without electronic resonances, the IIV-SFG spectra are dominated by the IR-active vibrational modes that are associated with Fermi resonance.[8,9] In contrast, the IIV-SFG process with electronic resonance allows for probing the mechanical and electronic coupling between any IR-active vibrational modes that are coupled through the electronic state.[6,7]

It is worthy emphasizing that previous IIV-SFG measurements were achieved using a femtosecond laser.[5-7,9] The broad band IR pulses allow to detect the vibrational modes that are enhanced by both Fermi resonance and electronic resonance. However, in our study, we used narrow band IR pulses ($\omega_{IR1} = \omega_{IR2}$) for the IIV-SFG process. The linewidth of the IR pulses is much smaller than the vibrational anharmonicity ($\Delta=\nu_{01}-\nu_{12}$) of many modes, as well as the energy difference between the Fermi resonant modes and the fundamental modes. In addition, a detailed analysis of IV-SFG and DIIV-SFG signals reveals that mainly the $\chi_{NL}^{(3)}$ contribution gives rise to the observed DIIV-SFG signals. Therefore, the vibrational modes associated with the Fermi resonance and the mechanical anharmonic coupling are out of our detection range, which makes the picosecond degenerate IIV-SFG (DIIV-SFG) allow identification of the vibrational modes that are coupled through the electronic states, which cannot be easily studied by linear vibrational spectroscopy and IV-SFG.

3. The molecular number contributing to the DIIV-SFG signal

The number of molecules contributing to the third-order response depends on the depth through which polarized and aligned molecules contribute to the DIIV-SFG process. In a crude approximation, the depth is determined by the coherence length l_c, which is defined as[13]

$$l_c = \frac{1}{k(\omega_{DIIV-SFG}) + k(\omega_{Vis}) + 2k(\omega_{IR})} = \frac{1}{2\pi\left(\frac{\sqrt{n(\omega_{DIIV-SFG})^2 - \sin^2\beta_{DIIV-SFG}}}{\lambda_{DIIV-SFG}} + \frac{\sqrt{n(\omega_{Vis})^2 - \sin^2\beta_{Vis}}}{\lambda_{Vis}} + \frac{2\sqrt{n(\omega_{IR})^2 - \sin^2\beta_{IR}}}{\lambda_{IR}}\right)} \quad \text{(S9)}$$

where β_i is the refracted angle. In our case, l_c = 42 nm at ω_{IR} = 1650 cm^{-1}. This means that DIIV-SFG technique is only contributed by the molecules in the surface distance of 42 nm.

4. IV-SFG and DIIV-SFG set up and experiments

The IV-SFG experimental setup is similar to that described in our earlier publications.[14] IV-SFG and DIIV-SFG spectra were collected by overlapping a visible and a tunable IR beam on the sample surface using a co-propagating configuration. The visible beam (ω_{Vis}) is set at a fixed wavelength of 532.1 nm while the IR beam (ω_{IR}) can be tuned from 1000 to 4300 cm^{-1}. The fundamental pulses have pulse duration of ~30 ps and a repetition rate of 10 Hz. The visible and

IR beams are spatially and temporally overlapped at the sample surface. The incidence angle at sample/air surface is 53° for the IR beam and 63° for the visible beam.

All of the SFG and IIV-TPF-FWM experiments were carried out at room temperature (24 ^{o}C) with a relative humidity of about 40%. The energy of visible beam and IR beam are both less than 120 μJ. IV-SFG and DIIV-SFG spectra from the molecules with polarization combinations ssp (s-polarized SFG output, s-polarized visible input, and p-polarized infrared input) were collected using the geometry of Fig. S1.

All IV-SFG and DIIV-SFG spectra were averaged 100 shots per data point and normalized by the intensities of the input IR and visible beams.

$$I_{IV-SFG}^{norm} = \frac{I_{IV-SFG}^{measure}}{I_{vis} I_{IR}} \tag{S10}$$

$$I_{DIIV-SFG}^{norm} = \frac{4 I_{DIIV-SFG}^{measure}}{I_{vis} I_{IR}^{2}} \tag{S11}$$

The spectra were fitted using Eq. (S12)

$$\chi_{eff}^{(2)}(\omega) = \chi_{NR}^{(2)} + \sum_{\upsilon} \frac{A_{\upsilon}}{\omega - \omega_{\upsilon} + i\Gamma_{\upsilon}} \tag{S12}$$

where A_{υ}, ω_{υ}, and Γ_{υ} are the strength, resonant frequency, and damping coefficient of the vibrational mode (ν), respectively.

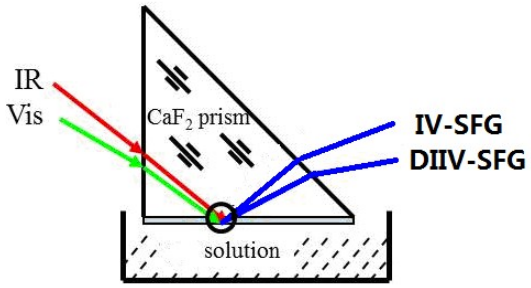

Fig. S1 Schematics of the IV-SFG and DIIV-SFG experimental geometry

4.1 The experiments of the film and flavin solution

A spin coater from Micaren Co., Ltd (Xiamen, China) was used to prepare flavin films on CaF_2 prisms from a 0.1 wt % solution at 2500 rpm. To study the influence of the FMN concentration on DIIV-SFG spectra, we prepared a series of FMN solution with the concentration of 0.01 mM, 0.02 mM, 0.05 mM, 0.1 mM, 0.5 mM, 1 mM, 3 mM, 5 mM, 10 mM, 15 mM and 20

mM. FMN was first dissolved in D_2O and sonicated for about 10 min before we carried out experiments. We collected the spectra using the same prism to keep the same experiment conditions. A magnetic stirrer was used to ensure a homogeneous concentration distribution of FMN in the D_2O. Before turning to another targeted concentration, the prism was washed using an ample amount of ultrapure water and tested using IV-SFG to confirm no FMN left.

4.2 The FMN/DMSO experiment

FMN were first dissolved in DMSO and sonicated for about 10 min to ensure mixing uniformity. The mixtures were stored for more than 24h in darkness in case of photolysis. Before the DIIV-SFG experiments, the mixtures were sonicated for about 10 min again to ensure uniformity. A magnetic stirrer was used during all the experiments.

4.3 The FMN/$CaCl_2$ solution experiment

Calcium chloride($CaCl_2$) was baked at around 500 °C for more than 6 h in order to remove the organic impurities. $CaCl_2$ was dissolved in D_2O (with the concentration of 2M) and sonicated for about 10 min. We first measured the DIIV-SFG spectra of FMN (5mM×2mL, dissolved in D_2O) with different polarization, and then we added 200uL $CaCl_2$ solution into the solution. Meanwhile, we collected the sspp DIIV-SFG spectra one by one until it reached equilibrium. A magnetic stirrer was used during all the experiments.

4.4 The redox reaction of FMN

Sodium hyposulfite ($Na_2S_2O_4$) was dissolved in D_2O (with the concentration of 500mM). Because $Na_2S_2O_4$ is easy to be oxidized, we used the fresh $Na_2S_2O_4$ in all experiments. Similar to the experiments of adding $CaCl_2$ solution into FMN, we first measured the DIIV-SFG spectra of FMN (10mM×2mL, dissolved in D_2O) with different polarization, and then we added 100uL $Na_2S_2O_4$ solution into the FMN solution. Immediately, we collected the sspp DIIV-SFG spectra one by one until it was entirely oxidized by the oxygen in the air. A magnetic stirrer was used during all the experiments.

5. Infrared spectra

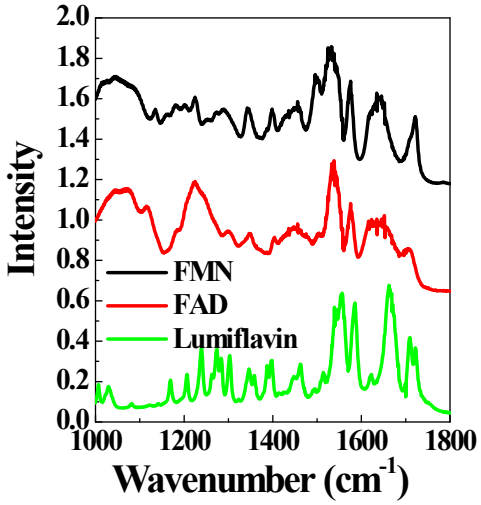

Fig. S2 Infrared spectra in the frequency range of 1100 - 1800 cm^{-1}.

6. The IIV-TPF-FWM spectra of lumichrome

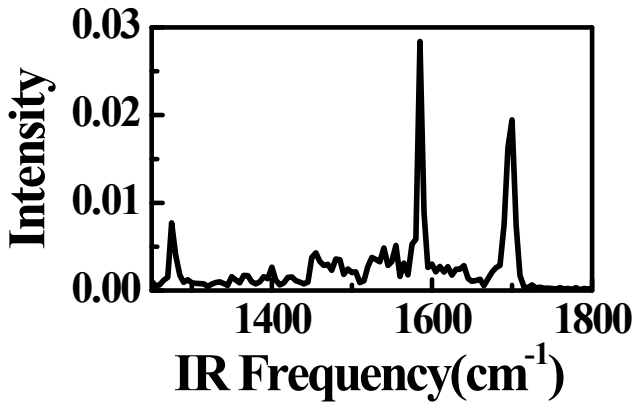

Fig.S3. The IIV-TPF-FWM sspp spectra of lumichrome.

The electronic absorption spectra of flavins have been well studied. It is found that the electronic absorption maxima of LF, RF, FMN and FAD in aqueous solution at ambient temperature occurs at about 450 nm and ~375 nm,[15,16] while electronic absorption maxima of lumichrome in ethanol solution at ambient temperature occurs at 339 nm and 384 nm.[17] Because the wave length of DII-SFG signal is about 455 nm, the DII-SFG processes in LF, RF, FMN and FAD are electronically resonant, but the one in lumichrome is far from the electronic resonance. Therefore, the DII-SFG signal of lumichrome was drastically reduced compared to the results of

LF, RF, FMN and FAD. This results demonstrated that the observed signals in Fig. 2B originated from the electronic resonance.

7. The discussion of DII-SFG signals of lumiflavin

As discussed in the main text, the intensity of 1550 cm^{-1} band is very sensitive to the flavin conformation. This band is associated with the formation of flavin dimer due to π-π stack interactions, which can cause a nonlinear enhancement of the electric field effect and thus benefit the local charge transfer interactions.[18] Here we prepared lumiflavin film using 0.1 wt % solution. In this condition, lumiflavin exists mainly as monomers, therefore, therefore, one the peak at ~1580 cm^{-1} was detected.

8. The influence of FMN concentration on the sspp DIIV-SFG spectra of FMN in D_2O solution

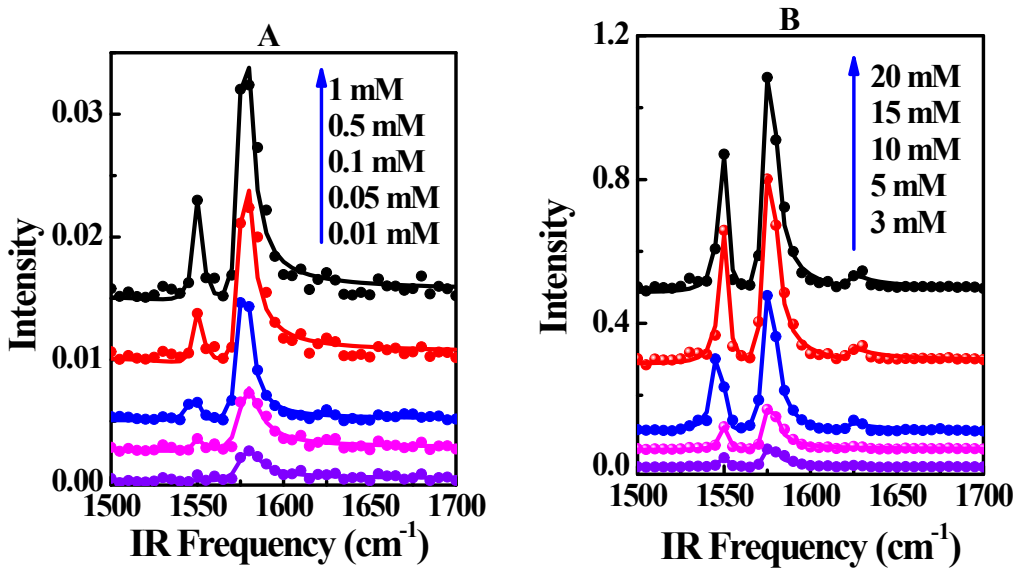

Fig. S4 The sspp DIIV-SFG spectra of FMN in D_2O solution with different concentration

Reference

1. Y. R. Shen, The Principles of Nonlinear Optics; John Wiley& Sons: New York, 1984.

2 F. G. Moore, G. L. Richmond, *Acc. Chem. Res.,* 2008, **41**, 739–748.

3 E. T. Castellana, P. S. Cremer, *Surf. Sci. Rep.,* 2006, **61**, 429–444.

4 A. G. Lambert, P. B. Davies, D. J. Neivandt, *Appl. Spectrosc. Rev.,* 2005, **40**, 103–145.

5 S. Gopalakrishnan, D. F. Liu, H. C. Allen, M. Kuo, M. J. Shultz, *Chem. Rev.,* 2006, **106***,* 1155–1175.

6 E.S. Boyle, N.A. Neff-Mallon, J.C. Wright, *J. Phys. Chem. A* 2013, **117**, 12401−12408.

7 E.S. Boyle, N.A. Neff-Mallon, J.D. Handali, J.C. Wright, *J. Phys. Chem. A,* 2014, **118**, 3112−3119.

8 E.S. Boyle, A.V. Pakoulev, J.C. Wright, *J. Phys. Chem. A,* 2013, **117**, 5578−5588.

9 M. Cho, *Phys. Rev. A,* **2000**, *61*, 023406.

10 M. Bonn, C. Hess, J. H. Miners, T. F. Heinz, H. J. Bakker, M. Cho, *Phys. Rev. Lett.,* 2001, **86**, 1566-1569.

11 R. S. Czernuszewicz, T. G. Spiro, *Inorganic Electronic Structure and Spectroscopy;* John Wiley & Sons: New York, 1999; pp 353.

12 T.G. Spiro, R. S. Czernuszewicz, *Resonance Raman Spectroscopy. In Physical Methods in Bioinorganic Chemistry*; L. Que, Ed., University Science Books: South Orange, NJ, 2000; pp 85.

13 X. Wei, S.C. Hong, X. Zhuang, T. Goto, Y.R. Shen, *Phys.Rev. E,* 2000, **62**, 5160-5172.

14 S. J. Ye, F. Wei, *Analyst,* 2011, **136**, 2489-2494.

15 G. R. Penzer, G. K. Radda, *Quart. Rev. London*, 1967, **21**, 43-65.

16 S. Salzmann, V. Martinez-Junza, B. Zorn, S.E. Braslavsky, M. Mansurova, C.M. Marian, W. Gartner, *J. Phys. Chem. A*, 2009, **113**, 9365-9375.

17 E. Sikorska, I. Khmelinskii, M.Hoffmann, I.F. Machado, L. F. V. Ferreira, K. Dobek, J. Karolczak,O A. Krawczyk, M. Insinska-Rak, M. Sikorski, *J. Phys. Chem. A* 2005, **109**, 11707-11714.

18 R. J. Stanley, H. Jang, J. Phys. Chem. A, 1999, **103**, 8976.